Title
CRACK MODELS FOR THE FAILURE OF ROCKS IN COMPRESSION

Authors
Kemeny, J.M.
Cook, N.G.W.

Publication Date
1986-12-01

LBL-25311

Lawrence Berkeley Laboratory
UNIVERSITY OF CALIFORNIA

EARTH SCIENCES DIVISION

Presented at the Second International Conference on Constitutive Laws for Engineering Materials: Theory and Applications, Tucson, AZ, January 5–8, 1987

Crack Models for the Failure of Rocks in Compression

J.M. Kemeny and N.G.W. Cook

December 1986

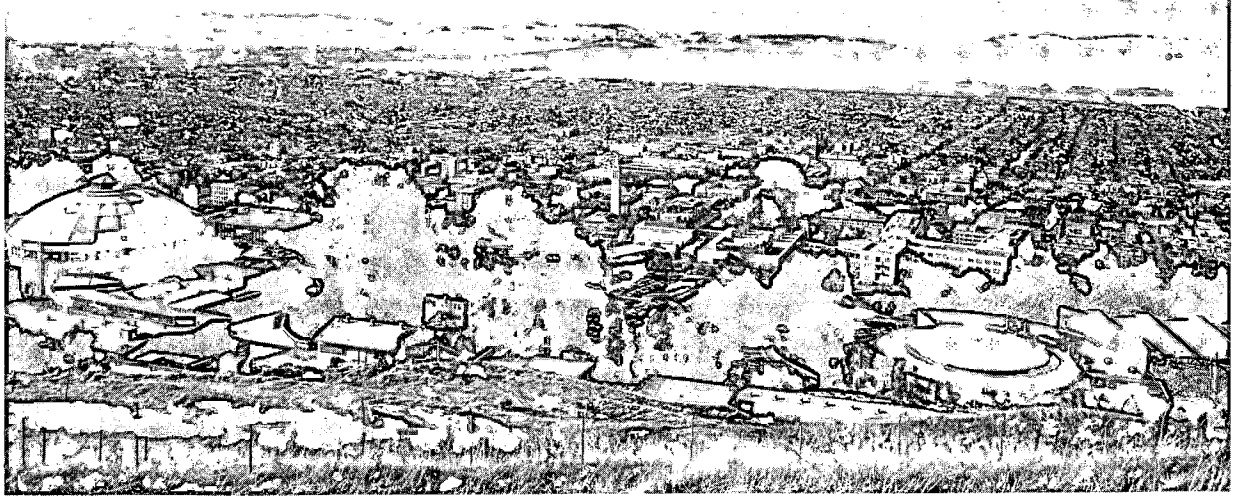

Prepared for the U.S. Department of Energy under Contract Number DE-AC03-76SF00098.

DISCLAIMER

CRACK MODELS FOR THE FAILURE OF ROCKS IN COMPRESSION

JOHN M. KEMENY AND NEVILLE G. W. COOK

Earth Sciences Division
Lawrence Berkeley Laboratory
and
Department of Materials Science and Mineral Engineering
University of California
Berkeley, California 94720

ABSTRACT

Fracture mechanics models are developed to analyze the post failure behavior of rocks under triaxial compression. We consider axially aligned 'sliding cracks' as a model for the axial growth of microcracks, and a collinear row of shear cracks at an angle to the direction of maximum compression, as a model for shear failure. It is found that the sliding crack model exhibits strain hardening and strain softening, while the shear crack model exhibits only strain softening. Also, we consider parallel columns of sliding cracks, and show that parallel interaction stabilizes the axial growth of cracks.

INTRODUCTION

When tested in triaxial compression, most rocks show a maximum axial compressive stress as a function of axial strain, referred to as the ultimate strength (Griggs and Handin, [1]). The ultimate strength for rocks is found to increase with increasing confining pressure, and to vary significantly between different rock types. Under sufficiently stiff testing conditions, rock can be deformed past the maximum compressive stress and into the 'post failure' region (Jaeger and Cook, [2]). Rocks can go unstable even under infinitely stiff (displacement controlled) testing conditions, if the stress strain curve in the post failure region passes through a vertical tangent and starts to loop back towards the origin. Using the notation of Wawersik and Fairhurst [3], class I and class II behavior refer to post failure behavior that is either stable or unstable under displacement controlled testing conditions, respectively. Wawersik [4] pioneered the use of unloading techniques to stabilize rocks exhibiting class II behavior. Wawersik used manual unloading, and similar results have been obtained recently using more sophisticated techniques such as servo-controlled unloading (Okubo and Nishimatsu, [5]). The reproducability of class I and II behavior for a given rock type (Wawersik and Brace, [6]) indicates that this behavior characterizes a material in the manner of the ultimate strength and elastic constants, and is therefore important from the standpoint of rock properties.

Laboratory studies have provided the groundwork for theoretical models based on microcracking to describe the nonlinear behavior of rocks under compressive stresses. It is now well known that the controlling mechanism for strain hardening and softening in brittle rocks is the growth, interaction, and coalescence of microcracks (Wawersik and Brace, [6]; Hallbauer et al., [7]; Tapponnier and Brace, [8]; Kranz, [9], and others). Recently, the use of high resolution scanning electron microscopes (SEM) has helped illuminate some of the mechanisms controlling the initiation and growth of microcracks, and the localization of deformation into macroscopic shear planes (Tapponnier and Brace, [8]; Kranz, [10]; Evans and Wong, [11]; Wong and Biegel, [12]; Wong, [13]). Mechanisms to generate the tensile stresses necessary for axial crack growth, that is, crack growth parallel to the direction of maximum compression, include shear along microcracks, stress concentrations around low aspect ratio

openings, and elastic moduli contrasts. Also, microprocesses leading to the formation of shear planes include microbuckling, kinking, rotation, and crushing.

Theoretical models have recently been developed to describe nonlinear rock deformation in terms of microcrack growth parallel to the direction of maximum compression (Stevens and Holcomb, [14]; Dey and Wang, [15]; Kachanov, [16,17]; Moss and Gupta, [18]; Costin, [19]; Nemat-Nasser, [20]; Zaitsev, [21]). The basis for many of these models is the 'sliding crack', shown in Figure 1a and first proposed by Brace et al. [22] and Fairhurst and Cook [23]. The sliding crack consists of a sliding 'shear crack', and sliding produces 'wing cracks' that emerge symmetrically from both ends of the sliding portions. Stress intensity factor solutions for various approximations to the sliding crack have been developed by Nemat-Nasser and Horii [24], Steif [26], Nemat-Nasser [20], and Zaitsev [21]. The sliding crack model is found to exhibit many of the features associated with microcracking in rocks (Wong, [13]), however, the microscopic studies to date reveal few instances where sliding cracks can actually be found. This could be due to the resolution of the microscopic studies, or the fact that samples are unloaded before SEM work is conducted. Also, it could be that other mechanisms for axial crack growth produce similar overall effects to those of sliding cracks. Nemat-Nasser [20] shows that cracks emanating from either a stiff inclusion or a circular void have many of the characteristics of the sliding crack. However, based on energy considerations, Wong [13] shows that some of the inelastic energy in rock deformation must be due to mechanisms such as the sliding crack.

In the next section, we consider axially aligned sliding cracks as a model for the axial growth of microcracks in rocks. Stress strain curves for this model are derived using the principles of linear elastic fracture mechanics. Our results show that the initial growth of the sliding cracks results in strain hardening, and the interaction with neighboring sliding cracks produces class I and class II strain softening. The effects of a confining stress are included, and the increase in the peak stress with increases in confining stress in the model are consistent with laboratory results. Our results are derived in analytic form, and therefore show the explicit dependence on the density and orientations of the initial shear cracks, the coefficient of friction, fracture toughness, and the elastic constants. These results are qualitatively similar to the results obtained by Costin [25,19] for a collinear row of axially growing cracks, where the driving force in his model is not due to shear sliding but rather linearly decreasing regions of tension. This similarity again indicates that several different mechanisms may be responsible for axial crack growth. Costin's results are not in analytic form, so the explicit dependence of the variables cannot be seen in his results.

The sliding crack model predicts that the ultimate failure of the material will occur by axial splitting, as the individual sliding cracks coalesce to form a macroscopic axial crack. Except for the case of triaxial compression with zero or small amounts of confining stress, the axial cracks do not in general grow to the ends of the sample, but rather, at some stage localization of deformation into one or two shear bands occurs. Kemeny and Cook [27] have developed analytical models for the shear deformation and stability of preexisting faults and joints. Nonlinear fault and joint deformation is due to the progressive failure of asperities along the contact surface, and Kemeny and Cook model this phenomena using collinear arrays of shear cracks that propagate in plane. Even though the mechanisms for shear localization are different than those for asperity failure, it is found that shear localization produces stress strain curves similar to those derived by Kemeny and Cook [27]. Therefore we develop this as a model for the shear failure of rocks in compression. Using this model, it is found that the shear failure model exhibits types I and II strain softening but no strain hardening. Also, both theoretical models and laboratory results show that shear localization and failure is in general a more stable process than axial crack growth, and therefore a mechanism must exist to stabilize the axial growth of cracks and allow the shear mechanisms to dominate. We look at one mechanism that may be responsible for the stabilization of the axially growing cracks, namely, the effect of parallel cracks.

AXIAL CRACK GROWTH

Here we consider a two dimensional (plane strain), linear elastic, isotropic, and homogeneous material containing a given configuration of sliding cracks, and subjected to axial and confining compressive stresses, σ_1 and σ_2, respectively. It is assumed that the sliding cracks are far enough away from the boundaries of the body such that the sliding cracks interact with each other but not with the boundaries of the body. The sliding portions of the cracks are closed and at an angle θ from horizontal; they resist sliding by a frictional force $\tau_f = \mu\sigma$, where σ is the normal stress acting on the sliding portions of the cracks, and μ is the coefficient of friction. In the actual sliding crack as proposed by Brace et al. [22], two curved wing cracks emerge from the ends of the sliding portions of the crack, and as the wing cracks grow they orient themselves in the direction of σ_1 , see Figure 1a. The sliding crack as shown in Figure 1a has been analysed in great detail (e.g., Horii and Nemat-Nasser, [28]), but from a computational point of view it is difficult to use , since stress intensity factor solutions for this configuration do not exist in analytic form. It is of interest, therefore, to seek approximate forms for the sliding crack model. One approximation to the sliding crack is shown in Figure 1b. Here the wing portions of the crack are straight and deviate from the sliding portion of the crack by an angle α, where α varies with the length of the wing crack. The stress intensity factor solution for this configuration has been given recently by Nemat-Nasser [20], as follows:

$$K_I = \frac{2\, l_0 \tau^* \sin\alpha}{\sqrt{\pi}(l + l^*)} - \frac{\sqrt{\pi} l}{2} \left[\sigma_1 + \sigma_2 + (\sigma_1 - \sigma_2) \cos 2(\alpha + \theta) \right] \qquad (1)$$

where

$$\tau^* = 1/2 \left[(\sigma_1 - \sigma_2) \sin 2\theta - \mu (\sigma_1 + \sigma_2 + (\sigma_1 - \sigma_2) \cos 2\theta) \right]$$

$$l^* = 0.27\, l_0$$

where $2l_0$ is the initial crack length, and α is chosen so as to maximize K_I (this equation differs slightly from that given in [20] due to sign convention and the angle θ being measured from vertical rather than horizontal). As the length of the wings increases, they will orient themselves in the direction of σ_1 , and this represents the long wing crack limit, as shown in Figure 1c. The stress intensity factor solution for this configuration under uniaxial compression has been given recently by Zaitsev [21], and is modified here to allow for σ_2 as follows:

$$K_I = \frac{2\, l_0 \tau^* \cos\theta}{\sqrt{\pi} l} - \sigma_2 \sqrt{\pi} l \qquad (2)$$

where τ^* is given in (1).

This stress intensity factor solution is computationally simple since it is based on the solution for a straight, axially oriented crack with symmetrically opposed point forces at the crack center, and can therefore be extended to the cases of parallel and collinear cracks. The long wing crack limit in Figure 1c, however, is not necessarily valid in our analysis, since it will be necessary in the derivations that follow to calculate the strain energy due to the cracks, which involves integrating the square of the stress intensity factor over the wing length from zero to some finite length. It turns out that the stress intensity factor solution in equation (1) quickly approaches the solution in equation (2) as the wing cracks extend, and therefore the configuration in Figure 1c is still a valid approximation in our analysis.

This will be demonstrated by calculating stress strain curves for a body containing a single sliding crack, using both the approximations in Figures 1b and 1c. We will then use the same approach as in the approximation in Figure 1c for bodies containing interacting cracks.

Stress strain curves for the crack configurations in this paper are calculated utilizing the principles of linear elastic fracture mechanics. We assume that the wing tips will extend when the mode I stress intensity factor, K_I, attains a value equal to the critical stress intensity factor, K_{IC}, also referred to as the fracture toughness, and assumed to be a constant. The critical value of the axial stress when $K_I = K_{IC}$ is referred to as the critical stress, σ_c. An elastic body containing sliding cracks will show linear axial stress-axial strain behavior under a fixed confining pressure up to the point where the wing cracks begin to extend. The slope of these linear 'loading' lines depends on the density, size, and orientations of the sliding portions of the cracks, the coefficient of friction, and the elastic constants. For certain values of the orientation of the sliding portions and of the relative amount of confining pressure, the sliding portions of the cracks will be locked, and for these cases, the loading lines have the same slope as those of a body containing no cracks. As the wing cracks extend, the slopes of the loading lines always decrease, but the critical stress, σ_c, can either increase or decrease depending on whether the stress intensity factor decreases or increases with an increase in the wing crack length. The stress strain curve is the locus of critical points for different loading line slopes, as described by Cook [29]. Strain hardening is the result of an increasing σ_c as the slope of the loading line decreases, and strain softening is the result of a decreasing σ_c as the slope of the loading line decreases. Also, class I softening is due to a slow decrease in σ_c with decreasing loading line slope, and class II softening results from a rapid decrease in σ_c with decreasing loading line slope. The fact that the slope of the loading line always decreases with an increase in the wing crack length merely reflects the softening effect that cracks produce on elastic bodies. In the formulation of the stress strain curve as described above, the stress strain curve is independent of the loading conditions, and therefore can be calculated without consideration for the stability of the system. Stability is governed by the interaction of the stress strain curve with the unloading stiffness of the testing system. Further details on stability are discussed in Kemeny and Cook [27,30].

The loading line for a configuration of sliding cracks is calculated using Castigliano's theorem (Sokolnikoff, [31]). Consider the system shown in Figure 2a. The body contains a single sliding crack and is under the action of three sets of stresses, axial and confining stresses σ_1 and σ_2, and a shear stress τ_f along the sliding portion of the crack. Here the body is assumed to be linearly elastic and the sliding crack surface is assumed to be frictionless, and τ_f represents the frictional stress that would exist due to the applied axial and confining stresses. By Castigliano's theorem, the axial displacement is given by:

$$\delta_P = \delta_P^e + \frac{\partial U_e}{\partial P} \qquad (3)$$

where δ_P^e represents the axial displacement that would occur in the uncracked body due to the applied stresses, U_e represents the elastic strain energy due to the sliding crack, and $P = 2w\sigma_1$, where 2w is the width of the body. The effective axial strain under the applied loads is then calculated by dividing the total displacement by the length of the body, 2b, and loading line solutions are produced when τ_f is replaced by a function of σ_1 and σ_2. We note here that the effective Poisson's ratio and the effective volume expansion due to a body with sliding cracks can be calculated using the lateral

displacement due to the applied stresses, which is calculated as above except the derivative of the strain energy is taken with respect to $Q = 2b\sigma_2$, rather than P.

The elastic strain energy due to the sliding cracks is the sum of of two components, that due to the initial shear cracks, and that due to the wing extension to the shear cracks. The strain energy due to initial shear cracks of length $2l_0$ has been calculated by Cook [29] and is given by:

$$U_e = \frac{\pi(\tau^* l_0)^2}{E}(1-\nu^2) \tag{4}$$

where E is Young's modulus. Using the reciprocal theorem, it can be shown that the strain energy due to the wing cracks is related to the effective shear stress along the sliding portions of the cracks. Looking closely at the stress intensity approximations for the sliding crack in equations (1) and (2),however, it is seen that they take into account only a component of the effective shear stress along the sliding surface, that component necessary to open or close a straight, axially aligned crack. Therefore, in order to use the approximations given in (1) and (2) to calculate strain energy, the normal relationship between stress intensity factors and strain energy (Irwin, [32]) is modified as follows:

$$U_e = \frac{(1-\nu^2)}{E\cos^2\theta}\int K_I^2\, dl \tag{5}$$

where the integral is over the wing crack length from zero to some finite length. For the approximation in Figure 1b, the integration in equation (5) must be evaluated numerically. For the approximation in Figure 1c, the strain energy can be calculated explicitly, and using equations (2), (3) and (4), the loading line solution becomes:

$$\varepsilon_1 = \frac{2\sin\theta\, l_0\,(1-\nu^2)}{Ewb}\left[\frac{\tau^*\pi\, l_0}{4\cos\theta} + \frac{\tau^* 2\, l_0\cos\theta}{\pi}\ln\frac{l}{l_0} - \sigma_2(l-l_0)\right] \tag{6}$$

Here we only consider the strain due to the sliding crack, i.e., the elastic strain due to the body with no cracks is left out. The critical stress, σ_c, for any loading line of a given slope is calculated by solving for σ_1 in equations (1) or (2) when $K_I = K_{Ic}$. The stress strain curve is then the locus of critical points on loading lines of different slopes. Normalized stress strain curves for the approximations in Figures 1b and 1c are presented in Figure 2b. The curves for these two cases are very similar and indicate that the simple approximation of Figure 1c is sufficiently accurate and useful because analytical solutions for this case are obtained. The main result of Figure 2b is that the sliding crack without crack interaction exhibits strain hardening.

We now extend this result to the case of an axially aligned column of sliding cracks, as shown in Figure 3a. Using the approach used in the approximations in Figure 1c, the stress intensity factor for an axially aligned column of sliding cracks is derived from the stress intensity factor solution for a collinear row of straight cracks, on each of which is a set of symmetric point forces at the crack center, and is given by [33]:

$$K_I = \frac{2l_0\tau^*\cos\theta}{\sqrt{(b\sin(\pi l/b))}} - \sigma_2\sqrt{(2b\tan(\pi l/b))} \tag{7}$$

Following the same procedure as for the non-interacting sliding crack, the loading line solution for the

axially aligned row of sliding cracks is given by:

$$\varepsilon_1 = \frac{4\sin\theta\, l_0\,(1-\nu^2)}{\pi E w b}\left[\frac{\tau^{*}\pi^{2} l_0}{8\cos\theta} + \tau^{*} l_0 \cos\theta \ln\frac{\tan(\pi l/b)}{\tan(\pi l_0/b)} - \sigma_2 b \ln\frac{\tan(\pi/4(1+l/b))}{\tan(\pi/4(1+l_0/b))}\right] \quad (8)$$

where again we consider only the strain due to the sliding cracks. The critical stress on each loading line is given by solving equation (7) for σ_1 when $K_I = K_{Ic}$, and the stress strain curve is the locus of critical points on loading lines of different slopes. Normalized stress strain curves for different values of σ_2 are presented in Figure 3b. The effects of crack interaction are clearly seen, as it causes both class I and class II types of strain softening in addition to initial strain hardening. Also, the model shows a strong increase in the peak stress with small increases in σ_2, which is in accord with laboratory data (e.g., Jaeger and Cook, [2]). The strong sensitivity to changes in σ_2 is due to the fact that the driving force for axial crack growth in our model comes from sliding at the center of the crack, whereas the stabilizing effect of σ_2 is felt over the whole crack surface. An important feature of this result is that it is only able to model convex strain softening slopes, even though laboratory testing results often exhibit low angle concave strain softening slopes. The results in Figure 3b are also in agreement with several of the other models for axial crack growth, namely the models of Costin [19] and Horii and Nemat-Nasser [28].

SHEAR FAILURE

Except at low confining stresses, rocks in general fail by a shear mechanism, and so in this section we investigate a simple model for shear failure. We consider the model shown in Figure 4a, which consists of a collinear row of cracks at an angle β to horizontal, under the action of axial and confining stresses, σ_1 and σ_2, and it is assumed that the cracks will grow in their own plane. Modifying the solution of Kemeny and Cook [27] for a collinear row of cracks under shear and normal stresses, the loading line solution for a row of cracks at an angle β under axial and confining stresses is given by:

$$\varepsilon_1 = \frac{4\tau^{*} b \cos\beta\,(1-\nu^2)}{\pi w E} \ln\cos(\pi l/2b) \quad (9)$$

where again the strain here is only that due to the sliding cracks. The stress intensity factor governing the configuration in Figure 4a is given by [33]:

$$K_{II} = \tau^{*}\,[2b\tan(\pi l/2b)]^{1/2} \quad (10)$$

Here the critical stress is calculated by solving for σ_1 when the energy release rate, G, given by:

$$G = \frac{(1-\nu^2)}{E} K_{II}^{2} \quad (11)$$

attains a critical value, G_c. Note that G_c here is related to the energy required to propagate the cracks in shear, as opposed to the fracture toughness, which is related to the energy required to propagate axially growing cracks in tension. Also, these shear driven cracks are an idealization for a complicated shearing process that involves microbuckling and kinking, and therefore the appropriate values of G_c for different rock types are difficult to determine. Rice [34]presents a methodology for determining G_c

from triaxial compression tests, and using this method, Wong [35] has determined G_c values for Westerly granite.

Normalized stress strain curves, calculated from values of the critical stress for loading lines of different slopes, are presented in Figure 4b for different values of confining stress. First of all, the curves in Figure 4b show that the shear model exhibits class I and class II types of strain softening, but does not exhibit strain hardening. Also, class I softening occurs over a larger portion of the stress strain curve and has slopes that are initially concave, compared with the very brief occurrence of class I softening with only convex slopes in the axial crack growth model. Both of these findings are supported by the laboratory work of Wawersik and Brace [6], Hallbauer et al. [7], and others, which show that strain hardening is associated with the initial axial growth of microcracks, and that shear faulting, when it occurs, usually results in low angle class I slopes that gradually approach a residual friction value. Class II behavior in shear faulting can occur, as it does in our shear models, but usually only after a much longer period of class I type behavior. The fact that the shear model can produce concave class I slopes indicates that the low angle softening slopes seen in laboratory results on many rock types may be due to a shearing type mechanism. The curves in Figure 4b show increasing strength with increasing confining stresses, but the rate of increase in strength with increasing confining stress is not as drastic as seen in the axial crack growth models. This is due to the fact that the driving force for shear crack growth is over the whole crack surface, and therefore the stabilizing effect of σ_2 is not as severe. This, therefore, gives a mechanism for the initiation of shear faulting at higher values of confining pressure as axial crack growth is stabilized.

STABILIZATION OF AXIAL CRACK GROWTH

One of the most interesting aspects of the shear results are the initial concave class I slopes that occur due to shear faulting, compared with the rapid progression to class II slopes in the case of axial crack growth. It may be expected that when two competing mechanisms are acting in a material, the more unstable of the two mechanisms should dominate. This indicates that a mechanism must exist to stabilize the axial growth of cracks, allowing the shear mechanism to occur, and preventing the axial cracks from growing to the ends of the sample. We briefly look at one mechanism that may be responsible for this stabilization.

We consider the effects of parallel rows of axially growing cracks. SEM studies (e.g., Evans and Wong, [11]) show very clearly that the spacing between axially growing cracks can be small compared with the length of the cracks. We consider a doubly periodic array of sliding cracks, Figure 5a, as a model that includes both parallel and collinear types of crack interaction. The stress intensity factor solution for a doubly periodic array of straight cracks, on which at the center of each crack is placed a symmetric set of point forces, has been solved by Chang [36]. This solution, however, is mathematically cumbersome, and therefore we seek approximations to the solution for the doubly periodic array of cracks. First we note that the doubly periodic array of cracks is equivalent to a single column of cracks with fixed displacement vertical boundaries. To approximate this configuration, we consider a single column of cracks under an axial stress, and apply the confining stress necessary to bring the lateral displacements back to zero. This solution can be calculated using Castigliano's theorem, and it is valid when the distance between parallel cracks, 2w, is large compared with the axial spacing between cracks, 2b. The stress intensity factor solution for a single axially aligned column of cracks with fixed lateral displacements, calculated as described above, is given by:

$$K_I = \frac{\tau^* 2\, l_0 \cos\theta}{\sqrt{(b\sin(\pi l/b))}} \left[1 - 2\sin(\pi l/2b) \frac{\ln \dfrac{\tan(\pi/4(1 + l/b)}{\tan(\pi/4(1 + l_0/b)}}{\dfrac{\pi w}{4b} + \ln \dfrac{\cos(\pi l_0/2b)}{\cos(\pi l/2b)}} \right] \qquad (12)$$

Stress strain curves based on this solution are presented in Figure 5b. Figure 5b shows that the effects of parallel cracks can indeed stabilize axial growth, causing class II strain softening slopes to turn back around to strain hardening slopes. Thus, parallel interaction can play an important role in promoting shear localization and failure, as opposed to further axial propagation.

CONCLUSIONS

The axial crack growth and shear failure models developed in this paper show many of the features seen in the post failure region of rocks tested in triaxial compression. It is found that the model for axial crack growth is much more sensitive to changes in confining pressure than the shear failure model, giving a mechanism for the onset of shear failure at larger confining pressures. Also, parallel crack interaction is found to stabilize the axial growth of cracks, allowing the more stable shear localization process to occur. More could be said about the models, in terms of their response to changes in material parameters, and additional calculations such as volume change and effective Poisson's ratio. It is found that using reasonable values for material parameters, the models predict actual material response very well.

ACKNOWLEDGEMENTS

The helpful comments by Russ Ewy, Victor Li , and Sia Nemat-Nasser are greatly appreciated. This work was supported in part by the Office of Geologic Repositories of the Office of Geologic Management of the US DOE under contract DE-AC03-76SF00098.. Also, one of the authors (J.K.) acknowledges support from the Jane Lewis graduate fellowship.

REFERENCES

1. Griggs, D. T., and Handin, J. *Observations of fracture and an hypothesis of earthquakes.* in Rock Deformation, Geol. Soc. Am. Mem., 79:347-364 (1960).
2. Jaeger, J. C. and Cook, N.G.W. Fundamentals of Rock Mechanics. Halsted Press, N.Y. (1976).
3. Wawersik, W.R., and Fairhurst, C. *A study of brittle rock fracture in laboratory compression experiments.* Int. J. Rock Mech. Min. Sci. 7:561-575 (1970).
4. Wawersik, W.R. *Detailed analysis of rock failure in laboratory compression tests.* Ph.D. Thesis. University of Minnesota (1968).
5. Okubo, S., and Nishimatsu, Y. *Uniaxial compression testing using a linear combination of stress and strain as the control variable.* Int. J. Rock Mech. Min. Sci. 22:323-330 (1985).
6. Wawersik, W. R. and Brace, W. F. *Post-failure behavior of a granite and diabase.* Rock Mech. 3:61-85 (1971).
7. Hallbauer, D.K., Wagner, H., and Cook, N.G.W. . *Some observations concerning the microscopic and mechanical behavior of quartzite specimens in stiff, triaxial compression tests.* Int. J. Rock Mech. Min. Sci. 10:713-726 (1973).
8. Tapponnier, P., and Brace, W.F. *Development of stress induced microcracks in Westerly Granite.* Int. J. Rock Mech. Min. Sci. 13:103-112 (1976).
9. Kranz, R. L. . *Crack-crack and crack-pore interactions in stressed granite.* Int J. Rock Mech. Min. Sci. 16:37-47 (1979).
10. Kranz, R. L. *Microcracks in rocks: a review.* Tectonophysics. 100:449-480 (1983).
11. Evans, B. and Wong, T.- f. *Shear localization in rocks induces by tectonic deformation.* In Mechanics of Geomaterials, edited by Z. Bazant, John Wiley and Sons (1985).
12. Wong, T.- f. and Biegel, R. *Effects of pressure on the micromechanics of faulting in San Marcos gabbro.* J. Struct. Geol. 7:737-749 (1985).
13. Wong, T.- f. *Geometric probability approach to the characterization and analysis o f microcracking in rocks.* Mechanics of Materials. 4:261-276 (1985).
14. Stevens, J. L. and Holcomb, D. J. *A theoretical investigation of the sliding crack model of dilatancy.* J. Geophs. Res. 85:7091-7100 (1980).
15. Dey, T. N. and Wang, C. *Some mechanisms of microcrack growth and interaction in compressive rock failure.* Int. J. Rock Mech. Mln. Sci. 18:199-209 (1981).
16. Kachanov, M. L. *A microcrack model of rock inelasticity part 1: frictional sliding on microcracks.* Mechanics of Materials. 1:19-27 (1982).
17. Kachanov, M. L. *A microcrack model of rock inelasticity part 2 :propagation o f microcracks.* Mechanics of Materials. 1:29-41 (1982).
18. Moss, W. C. and Gupta, Y. M. *A compressive model describing dilatancy and cracking in brittle rocks.* J. Geophys. Res. 87:2985-2998 (1982).
19. Costin, L. S. *Damage mechanics in the post failure regime.* Mech.of Mat. 4:149-160 (1985).
20. Nemat-Nasser, S. *Discussion of 'Geometric probability approach to the ... ' by T. Wong.* Mechanics of Materials. 4:277-281 (1985).
21. Zaitsev, Y. V. *Inelastic properties of solids with random cracks.* In Mechanics of Geomaterials, edited by Z. Bazant, John Wiley and Sons (1985).
22. Brace, W. F. , Paulding, B. W. , and Sholtz, C. *Dilitancy in the fracture of crystalline rocks.* J. Geophys. Res. 77:3939 (1966).
23. Fairhurst, C. and Cook, N. G. W. *The phenomenon of rock splitting parallel to a free surface under compressive stress.* Proc. First Cong. Int. Soc. Rock Mech, Lisbon. 1:687-692 (1966).
24. Nemat-Nasser, S., and Horii, H. *Compression-induced nonplanar crack extension with application to splitting, exfoliation, and rockburst.* J. Geophys. Res. 87:6805-6821 (1982).
25. Costin, L. S. *A microcrack model for the deformation and failure of brittle rock.* J. Geophys. Res. 88:9485-9492 (1983).
26. Steif, P. S. *Crack extension under compressive loading.* Eng. Fract. Mech. 20:463-473 (1984).
27. Kemeny, J. M., and Cook, N.G.W. *Frictional stability of heterogeneous surfaces in contact.* Proc. 27th U.S. Rock Mech. Symp. University, Alabama (1986).
28. Horii, H. and Nemat-Nasser, S. *Compression induced microcrack growth in brittle solids: axial splitting and shear failure.* J. Geophs. Res. 90: 3105-3125 (1985).
29. Cook, N. G. W. *The failure of rock.* Int. J. Rock Mech. Min. Sci. 2:389-403 (1965).
30. Kemeny, J. M., and Cook, N.G.W. *Effective moduli, non-linear deformation, and strength of a cracked elastic solid.* Int. J. Rock Mech. Min. Sci. 23:107-118 (1986).
31. Sokolnikoff, I. S. Mathematical Theory of Elasticity. 2nd edn, New York, McGraw Hill (1956).
32. Irwin, G. R. *Analysis of stresses and strains near the ends of a crack traversing a plate.* J. Appl. Mech.

24:361-364 (1957).
33. Sih, G.C. Handbook of Stress Intensity Factors. Inst. Fract. Solid Mech. Lehigh Univ., Bethlehem (1973).
34. Rice, J. R. *The mechanics of earthquake rupture.* In Physics of the Earth's Interior, edited by A. M. Dziewonski and E. Boschi, Italian Physical Society, Bologna, Italy (1980).
35. Wong, T.- f. *Shear fracture energy of Westerly granite from post-failure behavior.* J. Geophys. Res. 87:990-1000 (1982).
36. Chang, S. S. *The general solution of the doubly periodic cracks.* Eng. Frac. Mech. 18:887-893 (1983).

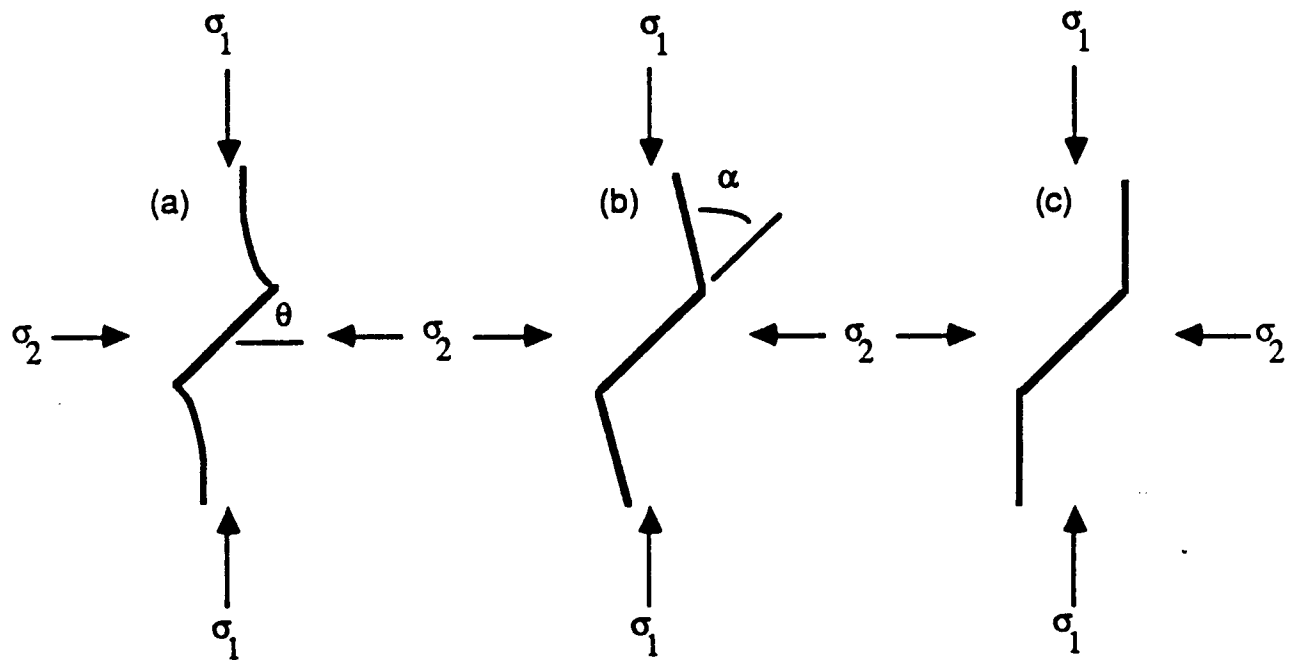

Figure 1. Sliding cracks with (a) curved wing cracks (b) straight wing cracks (c)long wing crack limit

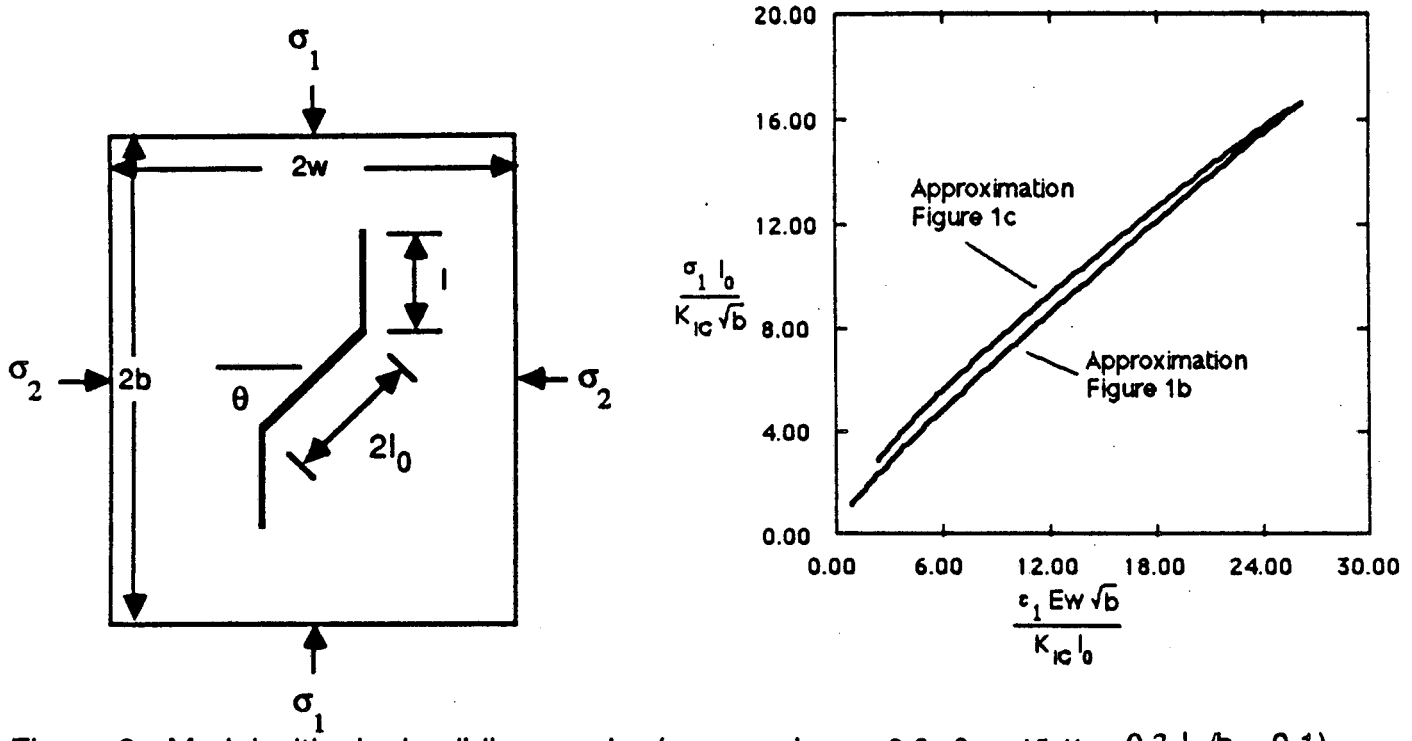

Figure 2. Model with single sliding crack. (assumed $\nu = 0.2$, $\theta = 45$, $\mu = 0.3$, $l_0/b = 0.1$)

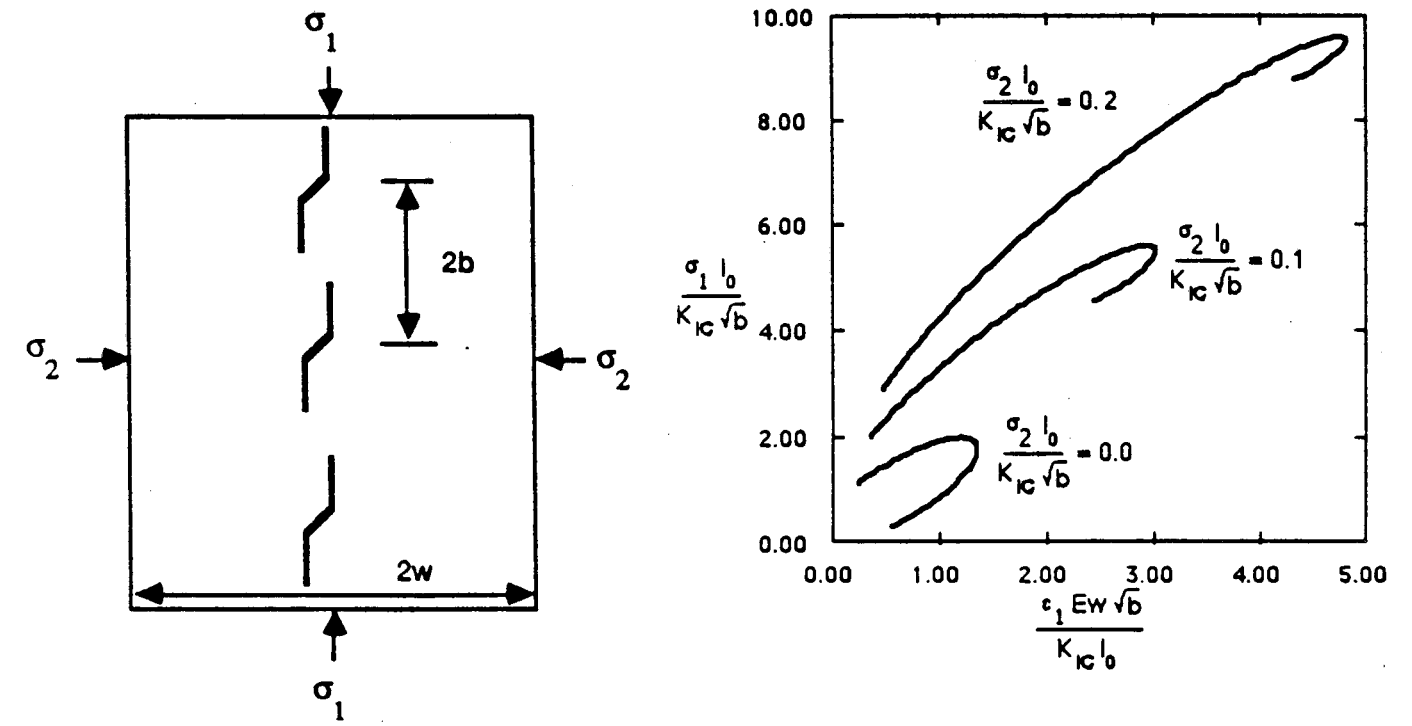

Figure 3. Model with axially aligned sliding cracks. (assumptions as in Figure 2)

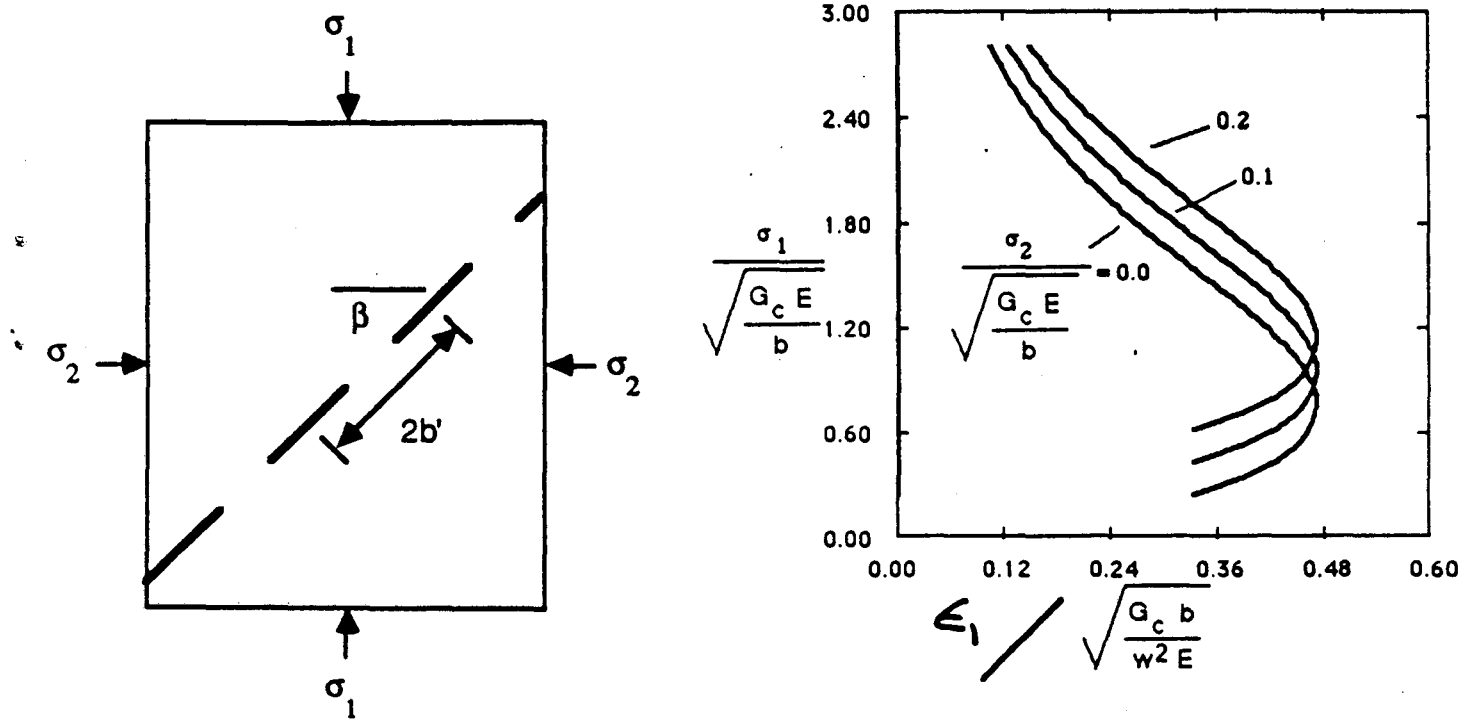

Figure 4. Model with collinear row of shear cracks. (assumptions as in Figure 2.)

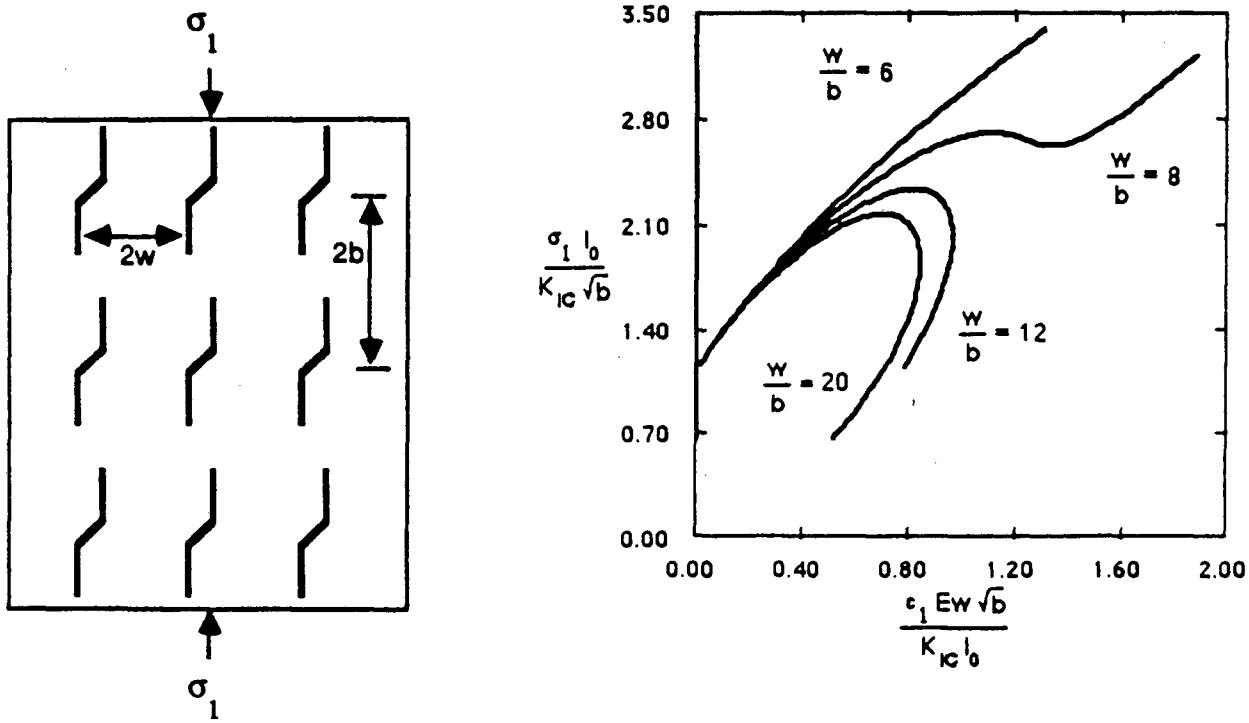

Figure 5. Model with doubly periodic array of sliding cracks (assumptions as in Figure 2)

LAWRENCE BERKELEY LABORATORY
OFFICE FOR PLANNING AND DEVELOPMENT
UNIVERSITY OF CALIFORNIA
BERKELEY, CALIFORNIA 94720